J Mater Sci: Mater Med (2013) 24:1853–1864
DOI 10.1007/s10856-013-4955-9

Characterisation, corrosion resistance and in vitro bioactivity of manganese-doped hydroxyapatite films electrodeposited on titanium

Yong Huang · Qiongqiong Ding · Shuguang Han · Yajing Yan · Xiaofeng Pang

Received: 24 February 2013 / Accepted: 7 May 2013 / Published online: 18 May 2013

Abstract This work elucidated the corrosion resistance and in vitro bioactivity of electroplated manganese-doped hydroxyapatite (MnHAp) film on NaOH-treated titanium (Ti). The NaOH treatment process was performed on Ti surface to enhance the adhesion of the MnHAp coating on Ti. Scanning electron microscopy images showed that the MnHAp coating had needle-like apatite crystals, and the approximately 10 μm thick layer was denser than HAp. Energy-dispersive X-ray spectroscopy analysis revealed that the MnHAp crystals were Ca-deficient and the Mn/P molar ratio was 0.048. X-ray diffraction confirmed the presence of single-phase MnHAp, which was aligned vertically to the substrate. Fourier transform infrared spectroscopy indicated the presence of phosphate bands ranging from 500 to 650 and 900 to 1,100 cm^{-1}, and a hydroxyl band at 3,571 cm^{-1}, which was characteristic of HAp. Bond strength test revealed that adhesion for the MnHAp coating was more enhanced than that of the HAp coating. Potentiodynamic polarisation test showed that the MnHAp-coated surface exhibited superior corrosion resistance over the HAp single-coated surface. Bioactivity test conducted by immersing the coatings in simulated body fluid showed that MnHAp coating can rapidly induce bone-like apatite nucleation and growth. Osteoblast cellular tests revealed that the MnHAp coating was better at improving the in vitro biocompatibility of Ti than the HAp coating.

Y. Huang · Q. Ding · S. Han · Y. Yan · X. Pang (✉)
Institute of Life Science and Technology, University of Electronic Science and Technology of China, No. 4 of Section 2, Jianshe North Road, Chengdu 610054, Sichuan, China
e-mail: pxf2012@yahoo.com.cn

Y. Huang
College of Lab Medicine, Hebei North University, Zhangjiakou 075000, China

X. Pang
International Centre for Materials Physics, Chinese Academy of Science, Shenyang 110015, China

1 Introduction

Metallic implants, such as commercially pure titanium (Ti), in dental and orthopaedic prostheses have achieved clear advantages in the last few years because of their biocompatibility, high strength, strong corrosion resistance and high elastic modulus [1]. To ensure their lasting clinical success, metallic implants are frequently covered with osteoconductive biomaterials, such as hydroxyapatite (HAp) ceramics [2–4]. HAp is one of the most effective bioceramics in the clinical repair of hard-tissue injury and illness [5]. HAp has been widely used clinically in various kinds of surgical treatments, namely, bone replacement material in orthopaedic surgery, craniofacial augmentation in plastic surgery and ossicular chain reconstruction in otorhinolaryngology surgical treatment [6].

However, the successful applications of HAp in implant material fields are limited by its comparatively slow rate of biological interactions. Thus, a demand exists to increase the success rate of HAp-coated medical implants. An effective means to increase osseointegration is to modify HAp chemically by doping with trace amounts of useful elements that exist in human bones [7]. Bioapatites are generally non-stoichiometric and involve some minor constituents such as positive ions (Mn^{2+}, Mg^{2+}, Sr^{2+}, Na^{+}, K^{+}, Cd^{2+}, Cr^{3+}, Pb^{4+} and Li^{+}) and/or anions (CO_3^{2-}, SO_3^{2-}, F^{-}, AsO_4^{3-} and VO_4^{3-}) [8]. These doped trace ions may modify the electrical charge and crystal structure of HAp, and have a potential effect on the biomaterials in a

physiological environment [8]. Manganese-doped HAp (MnHAp) has been studied, and this composite material greatly improves the quality and rate of bone repair in biocoating technology [9]. Mn^{2+} ions improve the ligand-binding affinity of integrins, a rather large family of receptors that regulates cell interactions with the extracellular matrix, and activate cellular adhesion [10–12]. Therefore, the presence of Mn^{2+} in HAp coating stimulates its interaction with the host bone tissue [13].

MnHAp coatings with excellent biocompatibility are prepared using various methods such as pulsed laser deposition [14, 15]. Cathodic electrodeposition (CED) is eliciting increasing attention as a superior method for the preparation of bioceramic coatings, inorganic composite coatings and organic protective coatings [16, 17]. The advantages of the CED technique are short formation time, simple preparation process, low-cost equipment, simple control of coating thickness, probability of fabricating onto porous substrates of complicated shapes, low process temperature, simple control of coating morphology and applicability for medical applications [18]. CED is ideally suitable for the deposition of ion-doped composite films [3, 7, 19, 20]. Therefore, applying the CED method is appropriate for the preparation of MnHAp coating.

In this study, we incorporate Mn^{2+} into electrodeposited HAp coatings to enhance the physiological stability, corrosion resistance and cell–biomaterial interactions. The Mn^{2+} of MnHAp coating may promote bone healing. The structural, mechanical and electrochemical behaviours of the coatings will also be discussed. This work will also study the cytocompatibility of the MnHAp coatings using mouse skull osteoblasts (MC3T3-E1).

2 Materials and methods

2.1 Electrodeposition of MnHAp film

Commercially pure Ti plates (99.9 % purity, Non-Ferrous Metals, Ltd., Baoji, China) of $10 \times 10 \times 1$ mm^3 size were designed as the substrates. The Ti substrate surface was finished gradually with SiC papers of different grits (400, 600, 800 and 1200). Then, the surface was cleaned with anhydrous ethanol, acetone and deionised water in an ultrasonic cleaner, followed by etching in 20 % v/v fluoric acid solution for about 30 s to eliminate the air-formed oxidised layer. The surface was subsequently ultrasonically washed in anhydrous ethanol and deionised water. Finally, the specimens were immersed in a stirred solution of 5 M NaOH at 65 °C for 24 h, ultrasonically cleaned in acetone and deionised water and dried at 80 °C for 1 h.

CED was carried out using an LK2005A electrochemical workstation (Tianjin, China). The Ti plate pretreated with NaOH solution was designated as the working electrode, a platinum sheet as the auxiliary electrode and a saturated calomel electrode (SCE) as the reference electrode. MnHAp coating was conducted in an electrolyte composed of 4.2×10^{-2} M $Ca(NO_3)_2$ (analytical grade), 2.5×10^{-2} M $NH_4H_2PO_4$ (analytical grade) and 3×10^{-4} M $Mn(NO_3)_2$ (analytical grade) under the following parameters: pH 4.3 ± 0.5, 0.85 mA cm^{-2} current density, 20–30 min and 65 ± 0.5 °C. After deposition, the samples were immersed in 1 M NaOH solution at 65 °C for approximately 2 h, washed in distilled water and then dried at 80 °C for 2 h. Then, the samples were sintered at 300 °C for 2 h in a vacuum environment. For comparison, pure HAp coating was designated as a control.

2.2 Coating characterisation

Scanning electron microscopy (SEM; JEOL JSM-6490LV, Japan) was used to observe the surfaces and cross-sections of the coatings. Quantitative elemental analysis of Ti, O, P, Ca and Mn was identified by energy-dispersive X-ray spectroscopy (EDS) (GENESIS 2000 XMS). A BEDE D1 SYSTEM X-ray diffraction (XRD) apparatus was used to analyse the crystal structure of the coating. The apparatus was operated with a Cu Kα radiation at 35 kV and 35 mA. The deposit powder scraped off from the Ti surface was employed in structural analysis conducted by Fourier transform infrared spectroscopy (FTIR, NICOLET NEXUS 670) using KBr pellet technology. A Tencor Alpha-Step IQ needle profilometer was used to measure film thickness.

2.3 Mechanical properties

The bond strength (BS) between the as-electrodeposited HAp coating and the Ti substrate was evaluated using an electronic universal testing machine, following the American Society for Testing Materials international standard F1044 [19–21]. Five replicates were conducted. The counter Ti substrate was attached to the surface of the HAp coating using epoxy. After heating in an oven at 120 °C for 2 h, the samples were tested for tensile strength at a constant speed of 0.001 cm min^{-1} until fracture. The adhesive BS was calculated as failure load/sample area (0.785 cm^2). For comparison, pure HAp coating (without NaOH pretreatment) was designated as a control.

2.4 Electrode polarisation test

The corrosion behaviour of the MnHAp coating in simulated body fluid (SBF) solution at 37 ± 0.5 °C was investigated by potentiodynamic polarisation test (electrochemical workstation, LK2005A, China). The platinum sheet was designed as auxiliary electrode, an SCE as

reference electrode and the uncovered or covered samples as working electrode with an exposed surface area of 100 mm^2. The polarisation curves of the MnHAp-, HAp-covered and bare samples in SBF were obtained at a scan rate of 10 mV s^{-1}. The specimens were soaked for 30 min to gain stable open-circuit potential.

2.5 SBF test

SBF was prepared using Kokubo and Takadama's formula [22], as shown in Table 1. MnHAp- and HAp-coated Ti were immersed in the centrifuge tubes containing 50 mL of SBF. SBF was kept at 37 ± 0.5 °C and was replaced every day. After immersion for 5 days, the samples were removed, cleaned by ultrapure water and air dried. Sample surfaces were characterised by SEM and EDS for investigation of in vitro bioactivity.

2.6 Cell test

Mouse calvarial cells (MC3T3-E1) purchased from West China School of Medicine were used to evaluate the osteoblastic cell response on specimens. The cells were cultured at 37 °C in a humidified 5 % CO_2 atmosphere in α-minimal essential medium (Hyclone) with 1 % penicillin/streptomycin (GIBCO) and 10 % fetal bovine serum (Hyclone). For the cell assay, the specimens were thoroughly sterilised in an autoclave at 121 °C for 25 min before the cell tests.

Cells (density of 5×10^4 cells mL^{-1}) were seeded on the coating to observe their morphology. After incubation for 1 day, cells were fixed with 2.5 % glutaraldehyde for approximately 2 h followed by dehydration with increasingly graded ethanol/water solutions (30, 50, 70, 80, 95 and 100 %). To observe cell morphology by SEM, the specimens were critical point dried using liquid CO_2 and then sputter-covered with gold film.

Table 1 The amount of materials needed to prepare 1,000 mL of SBF [22]

Salts	Amount	Purity (%)	Formula weight
NaCl	8.306 g	99.5	58.44
$NaHCO_3$	0.352 g	99.7	84.01
KCl	0.225 g	99.0	74.56
$K_2HPO_4{\cdot}3H_2O$	0.230 g	99.0	228.23
$MgCl_2{\cdot}6H_2O$	0.311 g	99.0	203.30
1 M HCl	40 mL	–	–
$CaCl_2$	0.293 g	99.0	110.98
Na_2SO_4	0.072 g	99.0	142.04
$(CH_2OH)_3CNH_2$ (Tris)	6.063 g	99.8	121.14
1 M HCl	0–0.2 mL	–	–

Cells were seeded at a density of 5×10^4 cells mL^{-1} onto the MnHAp- and HAp-coated Ti. The experiment was conducted in 24-well plates. Cells were incubated in a CO_2 incubator (5 % CO_2, saturated degree of humidity, 37 °C). The culture medium was renewed every 2 days. After 3 and 7 days of culture, the cells were incubated with a tetrazolium salt solution 3-[4,5-dimethylthiazol-2-yl]-2, 5-diphenyltetrazolium bromide (MTT) for 4 h at 37 °C. Then, the medium was removed and dimethyl sulfoxide was added into each well. After complete solubilisation of the deep-blue crystal of MTT formazan, cell viability was evaluated at 490 nm on a spectrophotometer. The cell proliferation rate was quantified by measuring the optical density (OD).

3 Results and discussion

3.1 Characterisation of the layer pretreated with NaOH solution

The XRD results reveal that the layer pretreated by NaOH was predominantly composed of Na_2TiO_3 (JCPDS File Card #50-0110) (Fig. 1a). The EDS spectrum in Fig. 1b shows the presence of O, Na and Ti. Notably, Ti was from the substrate, whereas the presence of a low Na concentration was due to the surface contamination of Na_2TiO_3 [23]. This result was parallel to the aforementioned XRD result. The NaOH pretreatment process leads to the formation of a thin surface layer of Na_2TiO_3 [23, 24]. Figure 2 shows the SEM images of Ti samples after NaOH pretreatment for 24 h. The Na_2TiO_3 layer formed smoothly and uniformly, with dense needle-like or flocculent crystal morphology [23]. NaOH treatment significantly enhanced the BS of bone to uncover Ti rods in rabbit femora [25]. An in vivo study [26] recently indicated the improved osseointegration of electrochemically prepared HAp on Ti–6Al–4V alloy because of a pretreatment consisting of NaOH immersion without ensuing heat treatment.

3.2 Characterisation of MnHAp coating

The formation of MnHAp coating was confirmed by the results of XRD, FTIR, EDS and SEM studies. The XRD patterns of the pure and MnHAp coatings are given in Fig. 3. Typical HAp peaks (JCPDS No. 09-0432) were identified in all patterns. After the appropriate hot alkaline pretreatment duration of 2 h, the main structure of the coating was transformed to HAp phase [27]. For the MnHAp coating (Fig. 3b), the unusual strong peak at 25.9° was assigned to the diffracted ray of MnHAp at the (0 0 2) plane, revealing a favoured apatite crystal growth orientation along the *c* axis on the Ti substrate. This result shows

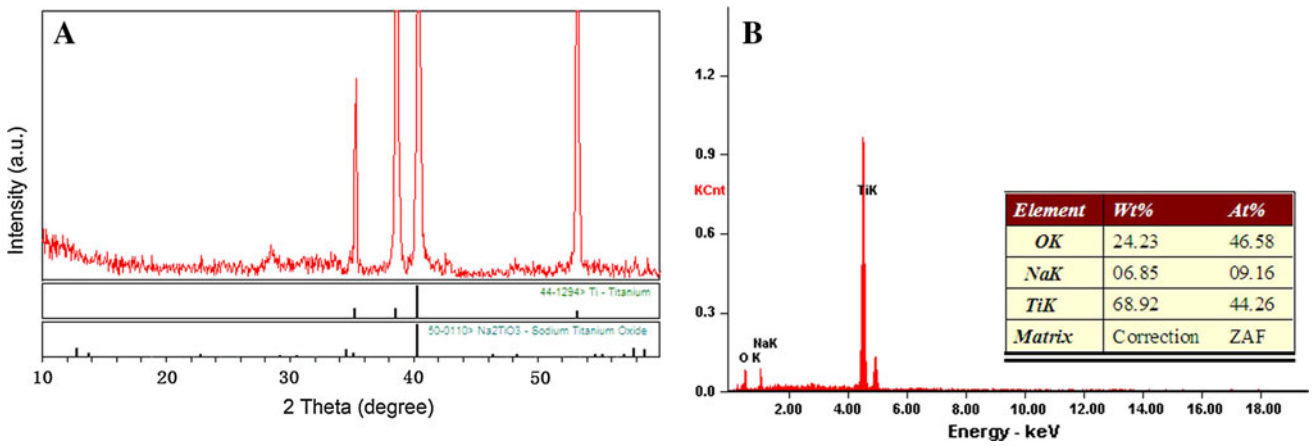

Fig. 1 **a** XRD pattern and **b** EDS elemental spectrum of the NaOH-treated Ti (Na_2TiO_3 layer)

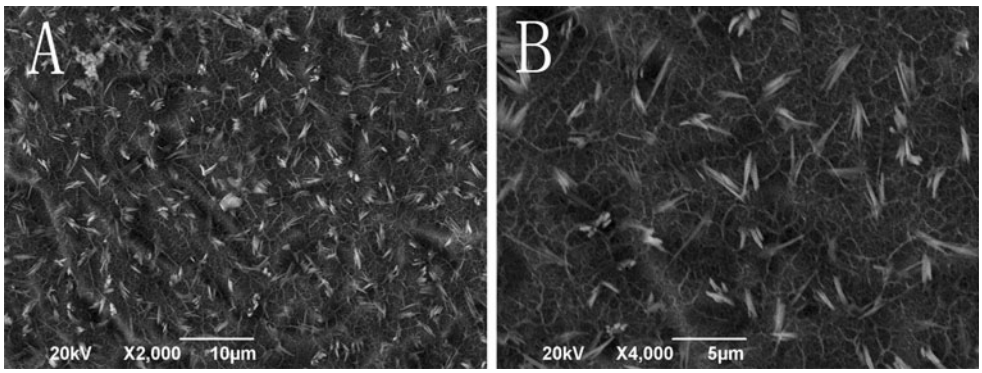

Fig. 2 SEM images of the surface of the NaOH-treated Ti (Na_2TiO_3 layer)

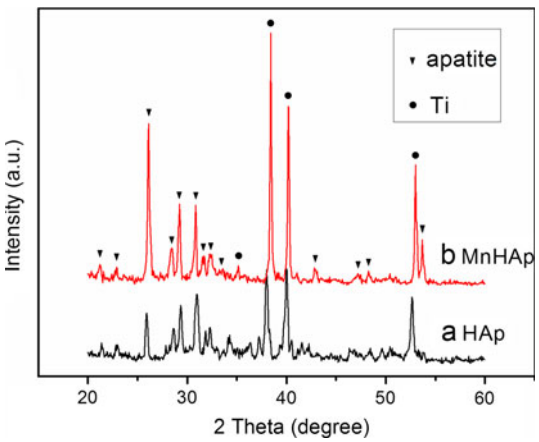

Fig. 3 XRD patterns of (*a*) the HAp- and (*b*) the MnHAp coatings

that the MnHAp crystal aligned perpendicularly to the substrate. Furthermore, the typical main peak of the crystal plane (21–30) seemed to be restrained.

Figure 4 shows the FTIR spectra of the film, which exhibited typical characteristics of the apatite crystals. For both HAp and MnHAp, the broad absorption band between 3,700 and 2,900 cm^{-1}, as well as the band at 1,651 cm^{-1}, corresponded to H_2O adsorbed on the surfaces; the absorption bands at 1093, 1034, 961, 603 and 562 cm^{-1} represent PO_4^{3-} [28]; the peak at 3,571 cm^{-1} was for –OH [29]; and the doublet at 1,461 and 1,421 cm^{-1} and the peak at 876 cm^{-1} could be attributed to carbonate ions replacing the phosphate [29], revealing that both films were carbonated HAp. The carbonate ions were from CO_2 in the air, which dissolved in the electrolyte solution and became involved in the reactions [30]. From a compositional perspective, bioapatites are always carbonated. The carbonated HAp with a deficient calcium group in the HAp structure is believed to be more attractive for clinical applications because bioactive ceramics improve osteoclast bone resorption due to their faster dissolution in acidic media [31, 32].

SEM analysis of the MnHAp layer revealed that this layer was smooth and dense. According to Fig. 5a, b, incorporating Mn^{2+} ions markedly increased the density, i.e., a relatively lower porosity than HAp coating (Fig. 5c, d). The presence of Mn^{2+} ions in the reaction solution restrained the precipitation, decreasing the dimensions of the needle aggregates [13]. According to the cross-sectional morphology of apatite layer shown in Fig. 6a, b, both HAp and MnHAp films formed smoothly and uniformly, with a thickness of nearly 10 μm without delamination

and/or cracking at the interface. The thick coating of 10 μm was suggested to be favourable for bone deposition [33, 34]. The crystallised needles aligned perpendicularly to the substrate (Fig. 6b), which was in agreement with the XRD results. The images of elemental mapping included coloured dots, and the dot density depended on the atomic number and the element concentrations [35]. From the EDS elemental mapping of Mn, Ca, P, Ti and O, the map showed uniform distribution of elements in the structure. Mn^{2+} ions were homogeneously distributed in the coating layer (Fig. 7).

EDS analysis clearly illustrated the presence and proportion of Mn, Ca, P, O and Ti in the HAp and MnHAp films, as shown in Fig. 8a, b. The EDS result of HAp-coated surface showed the presence of HAp components on the substrate (Fig. 8a). The chemical composition consisted of Ca, P, Ti and O. The Ca/P ratio was around 1.1, which was lower than 1.67 (the mole ratio of Ca to P of stoichiometric HAp). EDS analysis of MnHAp coating revealed the presence of Ti, Ca, P, O and Mn elements (Fig. 8b). The Ca/P and Mn/P molar ratios of the compounds formed on the Ti substrate were 1.13 and 0.048, respectively. This result suggests that MnHAp was Ca-deficient with a few Mn incorporations. Ca-deficient apatite is more beneficial to prompt the formation of new bone in vivo [7, 36]. The degree of Mn substitution $\times$ for MnHAp ($Ca_{10-x}Mn_x(PO_4)_6(OH)_2$) was about 1.63 ± 0.12, according to the EDS results (Fig. 8b). Gyorgy et al. [14] suggested that osteoblast proliferation and DNA replication on MnHAp ($x = 0.55$) are significantly higher than those on bare Ti.

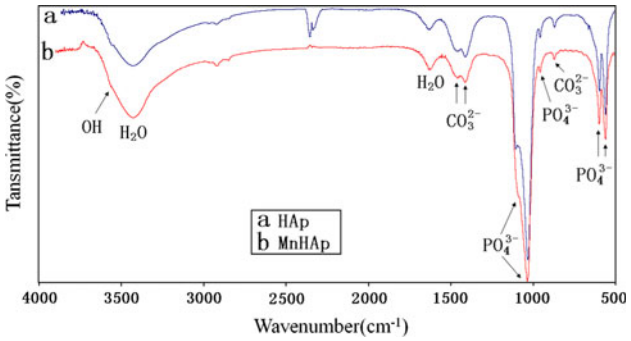

Fig. 4 FTIR spectra of the deposits scraped from the Ti substrate

3.3 Cathodic reaction and mechanism of deposition

The mechanism of CED may involve several chemical species and several types of reactions (electrochemical and chemical). First, the chemical formation of Na_2TiO_3 layer from an aqueous solution of NaOH is summarised as follows [37, 38]:

$$Ti + 3OH^- - 3e \rightarrow TiO_2 \cdot H_2O + \frac{1}{2}H_2, \quad (1)$$

$$TiO_2 \cdot H_2O + 2NaOH \rightarrow Ti(OH)_4 + Na_2TiO_3. \quad (2)$$

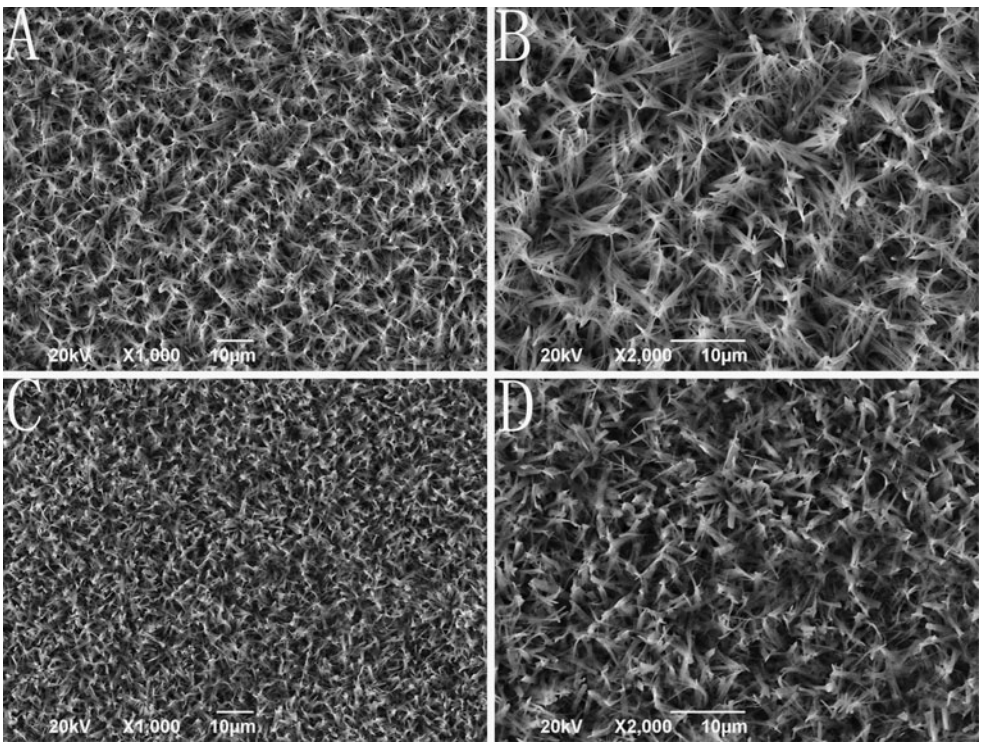

Fig. 5 SEM images of the **a**, **b** HAp- and the **c**, **d** MnHAp coatings

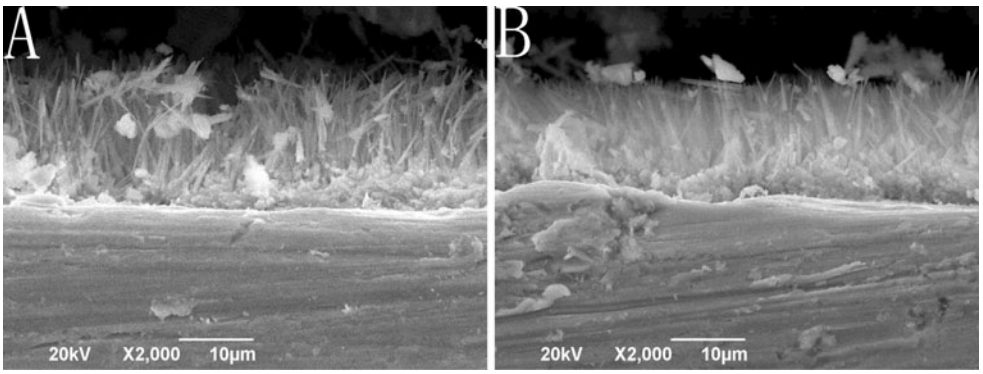

Fig. 6 Cross-section morphology of the **a** HAp- and the **b** MnHAp coatings

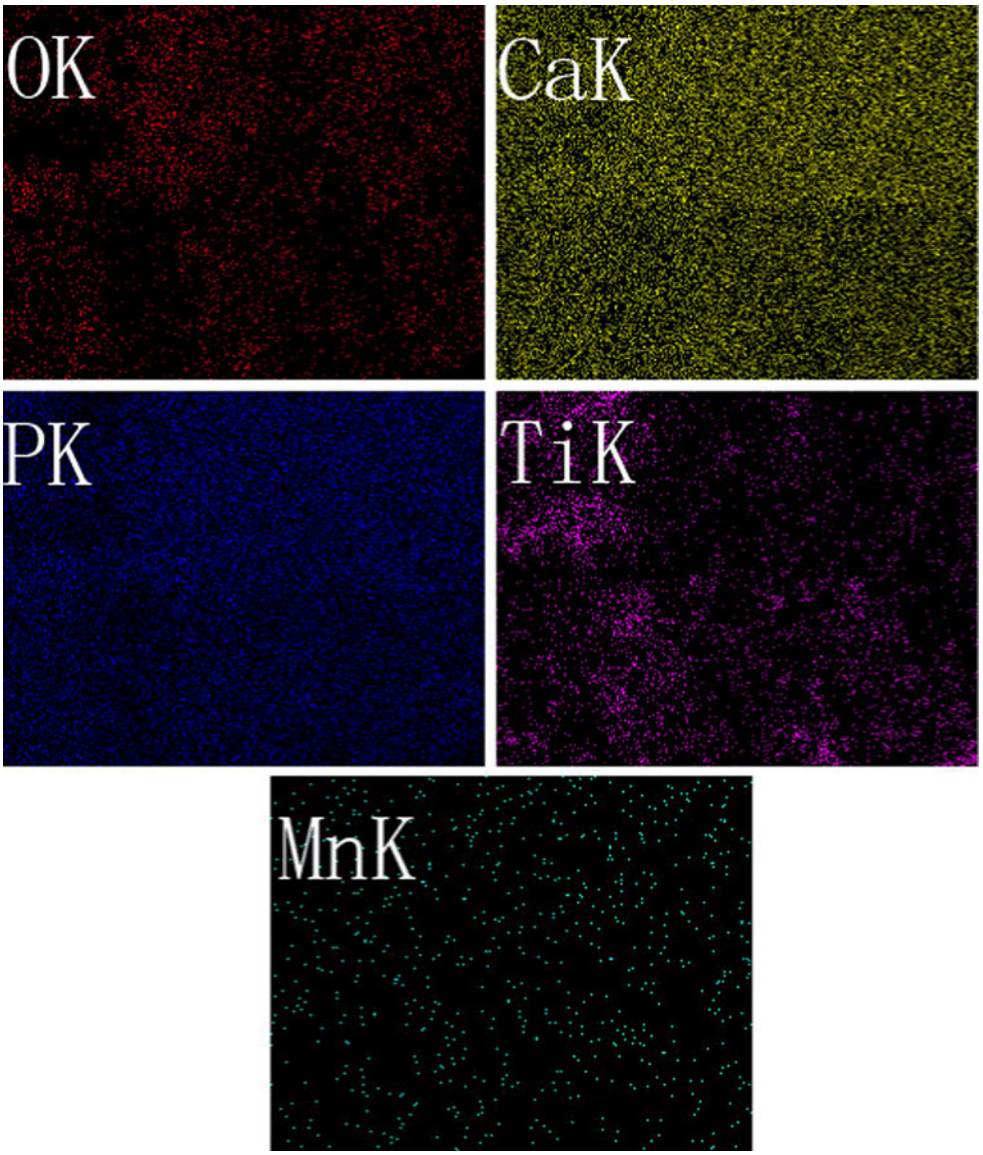

Fig. 7 Elemental mapping images of the MnHAp coating surface

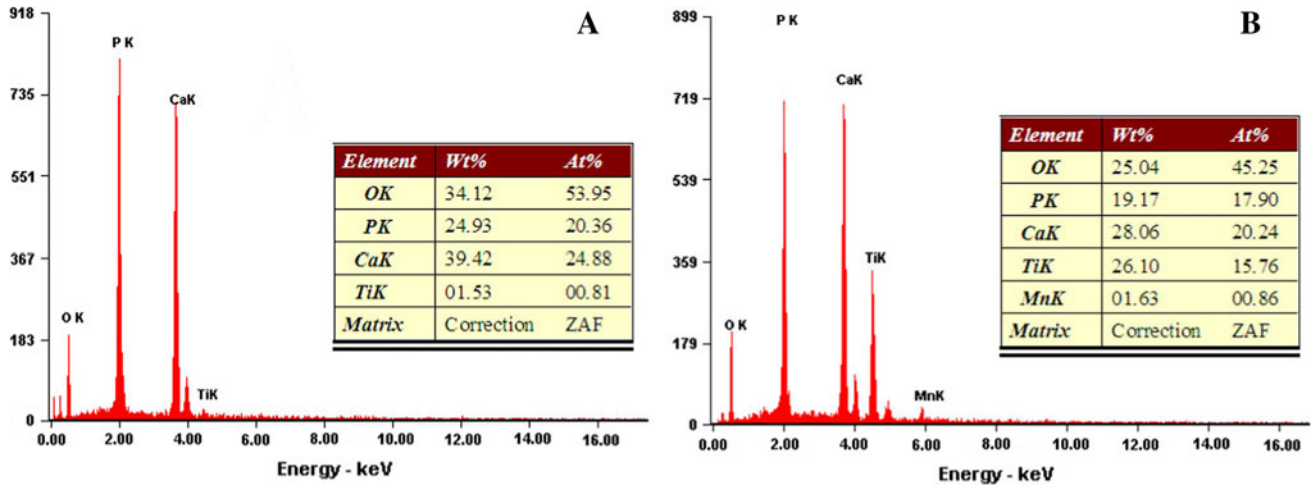

Fig. 8 EDS elemental spectrum of the **a** HAp- and the **b** MnHAp coatings

Second, the formation process of MnHAp layer can be described by a combination of several reactions, including acid–base reaction, electrochemical reactions, precipitation reaction and crystallisation process [19].

When a voltage is applied, the reactions at the Na_2TiO_3 film surface can be expressed as follows:

$$O_2 + 2H_2O + 4e^- \rightarrow 4OH^- \quad (3)$$

$$NO_3^- + H_2O + 2e^- \rightarrow 2OH^- + NO_2^- \quad (4)$$

$$H_2O + 2e^- \rightarrow H_2 + 2OH^-. \quad (5)$$

Reactions (3)–(5) result in a localised pH jump in the vicinity of the cathode, which leads to the following chemical reactions:

$$H_2PO_4^- + OH^- \rightarrow H_2O + HPO_4^{2-} \quad (6)$$

$$H_2PO_4^- + e^- \rightarrow HPO_4^{2-} + \frac{1}{2}H_2 \quad (7)$$

$$H_2PO_4^- \leftrightarrow HPO_4^{2-} + H^+. \quad (8)$$

Finally, HPO_4^{2-} combines with Ca^{2+} and Mn^{2+} to produce a $Ca_{1-x}Mn_xHPO_4{\cdot}2H_2O$ precipitate and deposits on the surface of the Na_2TiO_3 coating:

$$xMn^{2+} + (1-x)Ca^{2+} + HPO_4^{2-} \rightarrow Mn_xCa_{(1-x)}HPO_4 \cdot 2H_2O \quad (1 > x > 0). \quad (9)$$

When the alkaline treatment is applied to the coated samples, OH^- in the solution causes the following reaction [27]:

$$10Mn_xCa_{(1-x)}HPO_4 + 2OH^- \rightarrow Mn_{10x}Ca_{(10-10x)}(PO_4)_6(OH)_2 + 4PO_4^{3-} + 10H^+ \quad (1 > x > 0). \quad (10)$$

3.4 Evaluation of BS

The adhesion of HAp to the Ti substrate is significant for the implant to function suitably in physiological conditions. International standards demand that the BS value be at least 15 MPa [39]. The BS measured for the MnHAp film was 13.9 ± 3.7 MPa, nearly two times higher than 6.7 ± 2.1 MPa for pure HAp film, which provided predominantly high BS to meet the requirements of international standards [39]. This BS value of the MnHAp film was higher than that of the HAp film prepared by a traditional electrophoretic deposition process (11 MPa) [40]. Previous studies showed that NaOH pretreatment produces excellent BS between the HAp layer and the substrate [41]. The Na_2TiO_3 layer assists in HAp deposition because this layer can actively exchange ions with Ca^{2+} in the solution, thus transforming to $CaTiO_3$. $CaTiO_3$ represents a more beneficial surface for HAp formation than the other calcium phosphates, and acts as a binding layer between the Ti substrate and HAp [23]. In addition, the mismatch between the mechanical properties of the Ti substrate and the ceramic may be eliminated because of the increased density of the coating surface [42] and the presence of Mn^{2+} in the coating; the incorporation of Mn^{2+} into the lattice can strengthen the grain boundary cohesion by reducing the grain border energy [7, 8]. Thus, the MnHAp coating has favourable mechanical properties for use as an implant material under high bearing conditions.

3.5 Electrochemical corrosion test

Representative potentiodynamic polarisation curves obtained from the uncovered and covered Ti samples in SBF at 37 ± 0.5 °C are shown in Fig. 9. The corrosion potential

(E_{corr}) and the corrosion current density (I_{corr}) were calculated from the curves and listed as an inset in Fig. 9. The E_{corr} curves generally shifted to the positive potential side.

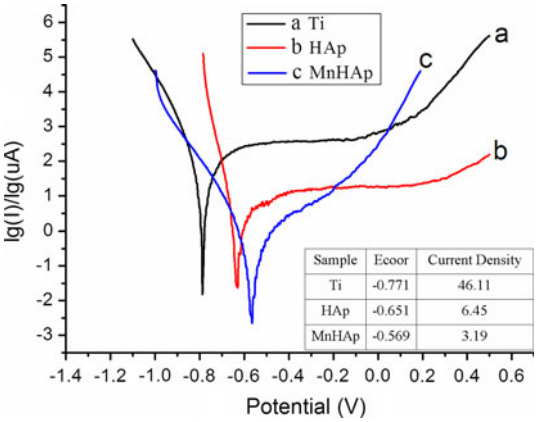

Fig. 9 The polarisation curves of the bare Ti and the Ti covered with coatings in SBF

E_{corr} of the HAp-coated Ti was about −0.651 V. Compared with the HAp coating, the MnHAp-coated sample exhibited a shift towards the positive side to −0.569 V. The MnHAp coating increased the corrosion resistance of the specimens by decreasing I_{corr}. For the HAp coating, I_{corr} was about 6.45 μA cm^{-2}, which decreased to 3.19 μA cm^{-2} for the MnHAp coating. I_{corr} for the sample covered with MnHAp film was about 14 times lower than that of the bare Ti (46.11 μA cm^{-2}). This result shows that the coatings improved the protection ability of the film, which served as a barrier layer against ionic diffusion. The MnHAp coating was electrodeposited on $NaTiO_3$-coated Ti substrate, consequently reducing the specific surface area because a denser and more uniform film was formed, as proven by the SEM image in Fig. 5. The reduced grain size had a significant function in promoting electron activity at the grain boundaries [43]. Thus, the surface became more electrochemically reactive, enhancing passivating ability, which resulted in the fast formation of a stable passive and mechanically strong film [44, 45]. These results

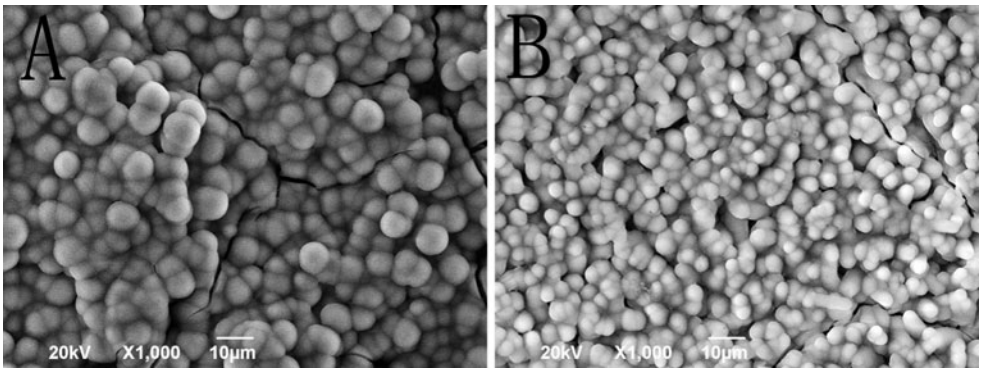

Fig. 10 SEM image of the apatite coating after immersion in SBF for 5 days: **a** HAp, **b** MnHAp

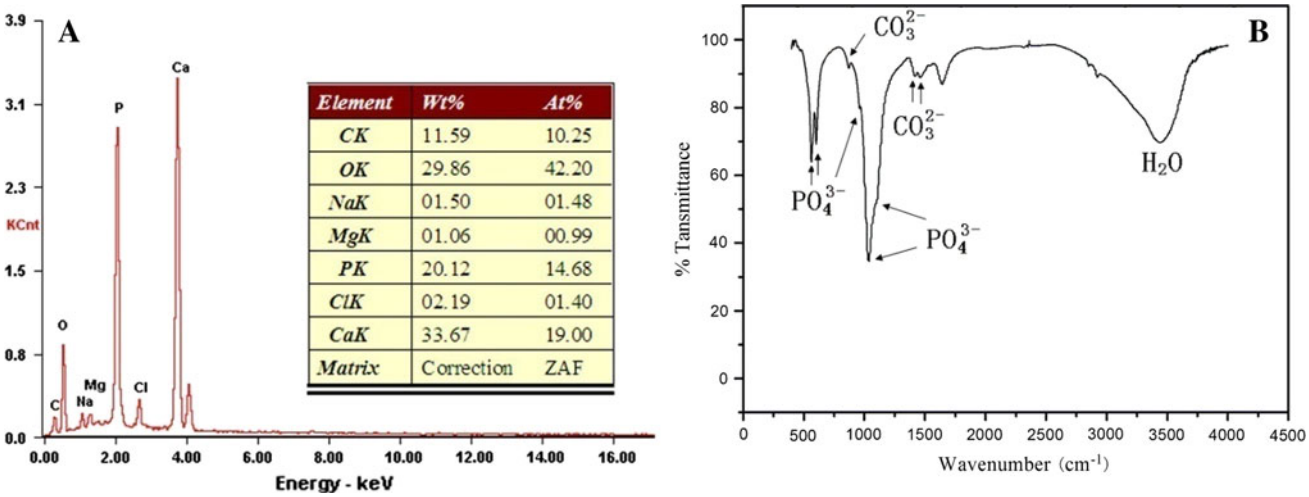

Fig. 11 **a** EDS elemental spectrum and **b** FTIR spectra of the MnHAp coating after immersion in SBF for 5 days

demonstrate that the MnHAp film acted as a protective barrier layer, which prevented ion diffusion and provided corrosion protection for the Ti substrate.

3.6 Immersion tests

The investigation of the biological activity of a biomaterial in SBF is an economical and valid method to study the in vivo bioactivity of the implant materials [22, 46]. As Fig. 10 shows, spheroid shapes were the typical morphology of apatite crystallised from SBF for 5 days. The results were confirmed by EDS analysis (Fig. 11a), which indicated an average mole Ca/P ratio of about 1.3 for specimens soaked in SBF than the initial specimens with Ca/P ratio of about 1.1 [47]. The new Mg, Na and Cl elements were detected in the spherical apatite (Fig. 11a). The FTIR spectra of the MnHAp-coated Ti, which was soaked in SBF for 5 days, are shown in Fig. 11b. Intense peaks between 850 and 1,200 cm^{-1} were assigned to the PO_4^{3-} group in apatite lattice. The bending and the stretching modes of PO_4^{3-} groups also appeared at 581 and 613 cm^{-1}. The absorption peaks of CO_3^{2-} group at 1,421 and 1,457 cm^{-1}, which replaced the phosphate groups in the apatite crystal structure, were detected. The sharpness of these peaks represented high crystallinity of apatite, as confirmed by SEM–EDS analysis [48].

The HAp- and MnHAp-covered Ti can induce bone-like apatite nucleation and growth on their surfaces from SBF

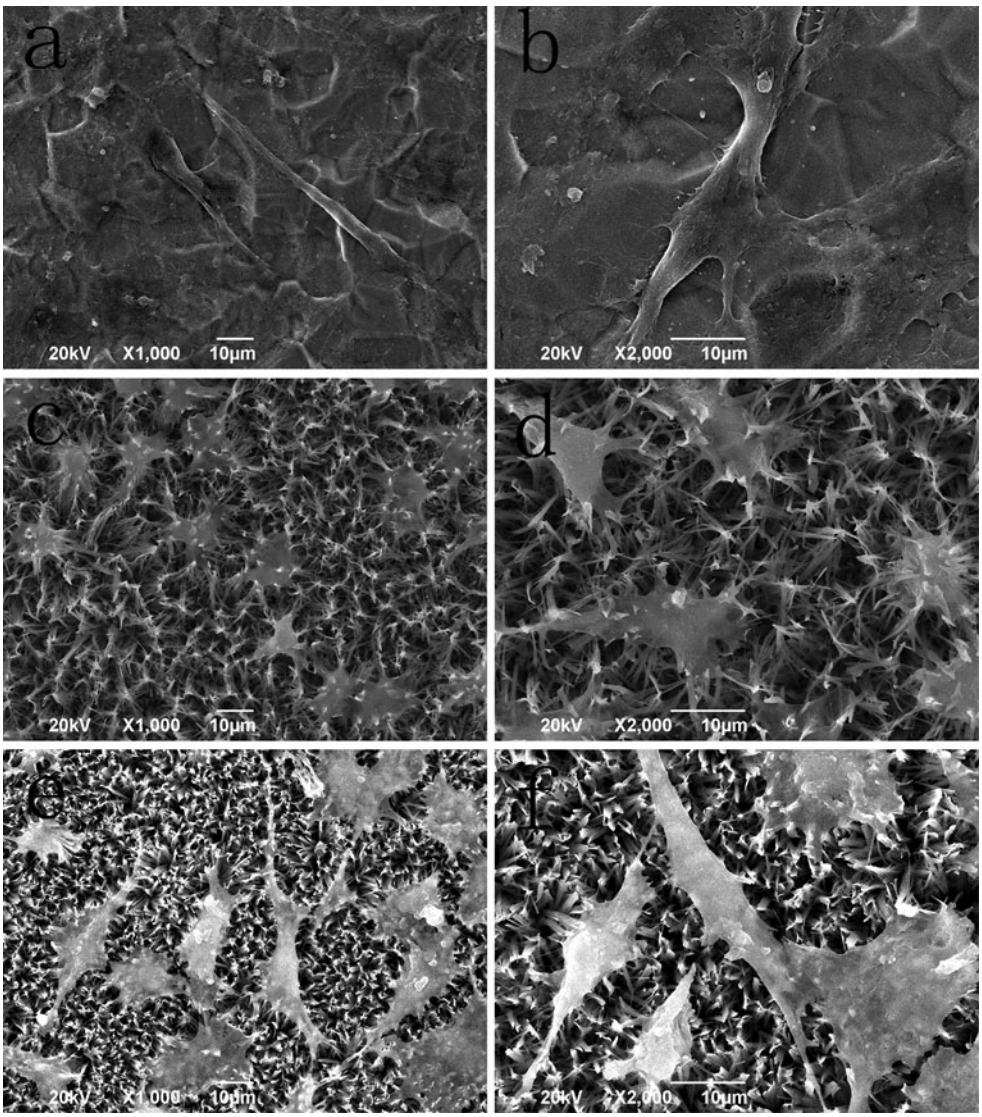

Fig. 12 SEM morphology of the MC3T3-E1 cells grown on bare Ti substrate (**a**), HAp- (**c**) and MnHAp coatings (**e**). The higher magnification images of the surface of the MC3T3-E1 cells grown on bare Ti substrate (**b**), HAp- (**d**) and MnHAp coatings (**f**)

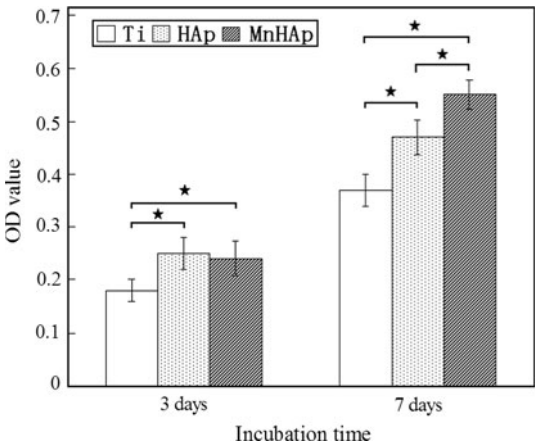

Fig. 13 OD measurements illustrating MC3T3-E1 cell proliferation on the ceramic coatings and bare Ti substrate after culturing for 3 and 7 days (one-way ANOVA, *★, $P < 0.05$)

after soaking for 5 days. The results indicated as follows [37, 38]:

$$\mathrm{Ti} + 3\mathrm{OH}^- - 3\mathrm{e} \rightarrow \mathrm{TiO_2} \cdot \mathrm{H_2O} + \frac{1}{2}\mathrm{H_2} \quad (11)$$

$$\mathrm{TiO_2} \cdot \mathrm{H_2O} + 2\mathrm{NaOH} \rightarrow \mathrm{Ti(OH)_4} + \mathrm{Na_2TiO_3}. \quad (12)$$

Second, the formation process of MnHAp layer can be described by a combination of several reactions that the HAp and MnHAp coatings have a higher rate of apatite formation than the plasma-sprayed HAp coating [47]. No apatite deposited on the surface of plasma-sprayed HAp-covered samples unless the soaking time was 10 days or more [47]. This result reveals that the HAp- and MnHAp-covered Ti have superior in vitro bioactivity in this work. The good bioactivity can be attributed to the effect of bone-like HAp and Ca deficiency on the coating. For MnHAp, the incorporation of Mn in the coating may also be an important factor [49].

3.7 Cytocompatibility analysis

Figure 12a–f show the representative SEM images of MC3T3-E1 cells after 24 h of culture on Ti substrate, MnHAp- and HAp coatings. The SEM results indicate that cells attached well onto the coatings and showed the typical osteoblast phenotype. As shown in Fig. 12c–f, the cells grown on the coatings had a polygon configuration and exhibited numerous filopodia and lamellipodia extensions. Osteoblasts on MnHAp appeared even more flattened and evenly spread across the coating surface [13]. This appearance suggested good cell viability on the MnHAp- and HAp films. By contrast, on the bare Ti surface (Fig. 12a, b), only a few cells were observed within a certain microscopic field. The cell density was lower than that on the apatite-coated specimens.

The degree (numbers) of cell proliferation was represented based on the absorbance value from MTT test after culturing for 3 and 7 days. The results are shown in Fig. 13. During the two periods, the cell numbers on bare Ti were significantly lower ($P < 0.05$) than those on the coated specimens, revealing that the MnHAp- and HAp coatings had higher biological activities than the bare Ti. No notable difference ($P > 0.05$) was found between the MnHAp- and HAp coatings after culturing for 3 days. By contrast, after 7 days, the cell numbers on the MnHAp coating were significantly higher ($P < 0.05$) than those on the HAp coating, suggesting that the MnHAp coating was better in stimulating cell proliferation. This result agreed with previous studies [12, 50, 51] showing that Mn^{2+}-containing HAp had excellent biological activity. Mn^{2+} was added to HAp because Mn^{2+} was linked to the activation of integrins [52], a family of receptors that regulate cell interactions with cell surface ligands and extracellular matrix. In the presence of Mn^{2+}, the ligand affinity of integrin increased and cell adhesion was stimulated. The salutary effect of MnHAp thin film was demonstrated in further studies [14, 15]. When osteoblasts were cultured on the surfaces of such thin films prepared on Ti substrates, the MnHAp coatings were better in facilitating cell proliferation, differentiation and metabolism. Furthermore, the beneficial effect of Mn was in agreement with the reported increase in serum levels of osteocalcin, discovered as a consequence of Mn supplementation in rats [53].

4 Conclusions

In this study, CED was successfully used for the synthesis of MnHAp coating, which had good corrosion resistance and in vitro bioactivity. The MnHAp crystals were needle-like and Ca-deficient with a few Mn incorporations. The addition of Mn^{2+} into HAp significantly reduced the porosity, and the coating became significantly denser. The MnHAp crystal was preferentially arranged in the (002) direction. The BS of the MnHAp coating obtained on the NaOH-treated Ti was about twice as large as that of the HAp coating, which possibly resulted from the collaborative effect of dense MnHAp crystallites and the intermediate Na_2TiO_3. The MnHAp film exhibited higher corrosion resistance in SBF than the HAp coating. SBF immersion tests indicated that MnHAp-coated Ti had good in vitro bioactivity. The incorporation of Mn and Ca deficiency in the coating was the main reasons for the good bioactivity. The in vitro cellular biocompatibility tests revealed that the MnHAp coating was more effective in improving the cytocompatibility of Ti in vitro than the HAp coating. The MnHAp film is a promising material to fabricate biomedical implants with advanced functionality.

The method developed in this investigation can be used to fabricate other ion-doped films for various applications.

Acknowledgments This work was supported by the National Basic Research Program of China ("973" Program, No. 2011CB503700), the outstanding doctoral academic projects of the University of Electronic Science and Technology of China (No. YBXSZC 20131042) and the Natural Science Foundation of China (No. 61071026). The authors thank Xuexin Wang for his assistance in the revision of the manuscript.

References

1. Gad El-Rab SMF, Fadl-allah SA, Montser AA. Improvement in antibacterial properties of Ti by electrodeposition of biomimetic Ca–P apatite coat on anodized titania. Appl Surf Sci. 2012;261:1–7.
2. Li L, Lu X, Meng YZ, Weyant CM. Comparison study of biomimetic strontium-doped calcium phosphate coatings by electrochemical deposition and air plasma spray: morphology, composition and bioactive performance. J Mater Sci Mater Med. 2012;23:2359–68.
3. Bir F, Khireddine H, Touati A, Sidane D, Yala S, Oudadesse H. Electrochemical depositions of fluorohydroxyapatite doped by Cu^{2+}, Zn^{2+}, Ag^{+} on stainless steel substrates. Appl Surf Sci. 2012;38:4885–93.
4. Yanovska A, Kuznetsov V, Stanislavov A, Danilchenko S, Sukhodub L. Calcium–phosphate coatings obtained biomimetically on magnesium substrates under low magnetic field. Appl Surf Sci. 2012;258:8577–84.
5. Shepherd JH, Shepherd DV, Best SM. Substituted hydroxyapatites for bone repair. J Mater Sci Mater Med. 2012;23:2335–47.
6. Tan F, Naciri M, Dowling D, Al-Rubeai M. In vitro and in vivo bioactivity of CoBlast hydroxyapatite coating and the effect of impaction on its osteoconductivity. Biotechnol Adv. 2012;30:352–62.
7. Li HJ, Zhao XN, Cao S, Li KZ, Chen MD, Xu ZW, et al. Na-doped hydroxyapatite coating on carbon/carbon composites: preparation, in vitro bioactivity and biocompatibility. Appl Surf Sci. 2012;263:163–73.
8. Paluszkiewicz C, Slosarczyk A, Pijocha D, Sitarz M, Bucko M, Zima A, et al. Synthesis, structural properties and thermal stability of Mn-doped hydroxyapatite. J Mol Struct. 2010;976:301–9.
9. Mayer I, Cuisinier FJG, Gdalya S, Popov I. TEM study of the morphology of Mn^{2+}-doped calcium hydroxyapatite and β-tricalcium phosphate. J Inorg Biochem. 2008;102:311–7.
10. Sopyan I, Ramesh S, Nawawi NA, Tampieri A, Sprio S. Effects of manganese doping on properties of sol–gel derived biphasic calcium phosphate ceramics. Ceram Int. 2011;37:3703–15.
11. Park JW, Kim YJ, Jang JH. Surface characteristics and in vitro biocompatibility of a manganese-containing titanium oxide surface. Appl Surf Sci. 2011;258:977–85.
12. Li Y, Widodo J, Lim S, Ooi CP. Synthesis and cytocompatibility of manganese(II) and iron(III) substituted hydroxyapatite nanoparticles. J Mater Sci. 2012;47:754–63.
13. Bracci B, Torricelli P, Panzavolta S, Boanini E, Giardino R, Bigi A. Effect of Mg^{2+}, Sr^{2+}, and Mn^{2+} on the chemico-physical and in vitro biological properties of calcium phosphate biomimetic coatings. J Inorg Biochem. 2009;103:1666–74.
14. Gyorgy E, Toricelli P, Socol G, Iliescu M, Mayer I, Mihailescu IN, et al. Biocompatible Mn^{2+}-doped carbonated hydroxyapatite thin films grown by pulsed laser deposition. J Biomed Mater Res A. 2004;71A:353–8.
15. Bigi A, Bracci B, Cuisinier F, Elkaim R, Fini M, Mayer I, et al. Human osteoblast response to pulsed laser deposited calcium phosphate coatings. Biomaterials. 2005;26:2381–9.
16. Erakovic S, Veljovic D, Diouf PN, Stevanovic T, Mitric M, Janackovic D, et al. The effect of lignin on the structure and characteristics of composite coatings electrodeposited on titanium. Prog Org Coat. 2012;75:275–83.
17. Song YW, Shan DY, Han EH. A novel biodegradable nicotinic acid/calcium phosphate composite coating on Mg–3Zn alloy. Mater Sci Eng C. 2013;33:78–84.
18. Djosic MS, Panic V, Stojanovica J, Mitric M, Miskovic-Stankovic VB. The effect of applied current density on the surface morphology of deposited calcium phosphate coatings on titanium. Colloid Surf A. 2012;400:36–43.
19. Huang Y, Yan YJ, Pang XF. Electrolytic deposition of fluorine-doped hydroxyapatite/ZrO_2 films on titanium for biomedical applications. Ceram Int. 2013;39:245–53.
20. Huang Y, Han SG, Pang XF, Ding QQ, Yan YJ. Electrodeposition of porous hydroxyapatite/calcium silicate composite coating on titanium for biomedical applications. Appl Surf Sci. 2012. doi: 10.1016/j.apsusc.2013.01.187.
21. Maleki-Ghaleh H, Khalili V, Khalil-Allafi J, Javidi M. Hydroxyapatite coating on NiTi shape memory alloy by electrophoretic deposition process. Surf Coat Technol. 2012;208:57–63.
22. Kokubo T, Takadama H. How useful is SBF in predicting in vivo bone bioactivity? Biomaterials. 2006;27:2907–15.
23. Blackwood DJ, Seah KHW, Han EH. Electrochemical cathodic deposition of hydroxyapatite: improvements in adhesion and crystallinity. Mater Sci Eng C. 2009;29:1233–8.
24. Wang CX, Wang M, Zhou X. Nucleation and growth of apatite on chemically treated titanium alloy: an electrochemical impedance spectroscopy study. Biomaterials. 2003;24:3069–77.
25. Nishiguchi S, Fujibayashi S, Kim HM, Kokubo T, Nakamura T. Biology of alkali- and heat-treated titanium implants. J Biomed Mater Res A. 2003;67:26–35.
26. Lakstein D, Kopelovitch W, Barkay Z, Bahaa M, Hendel D, Eliaz N. Enhanced osseointegration of grit-blasted, NaOH-treated and electrochemically hydroxyapatite-coated Ti–6Al–4V implants in rabbits. Acta Biomater. 2009;5:2258–69.
27. Zhao QM, Guo X, Dang XQ, Hao JM, Lai JH, Wang KZ. Preparation and properties of composite MAO/ECD coatings on magnesium alloy. Colloid Surf B. 2013;102:321–6.
28. Chen JD, Wang YJ, Wei K, Zhang SH, Shi XT. Self-organization of hydroxyapatite nanorods through oriented attachment. Biomaterials. 2007;28:2275–80.
29. Joseph Nathanael A, Mangalaraj D, Chi Chen P, Ponpandian N. Enhanced mechanical strength of hydroxyapatite nanorods reinforced with polyethylene. J Nanopart Res. 2011;13:1841–53.
30. Wang J, Shaw LL. Morphology enhanced low temperature sintering of nanocrystalline hydroxyapatite. Adv Mater. 2007;19:2364–9.
31. Zima A, Paszkiewicz Z, Siek D, Czechowska J, Slosarczyk A. Study on the new bone cement based on calcium sulfate and Mg, CO_3 doped hydroxyapatite. Ceram Int. 2012;38:4935–42.
32. Morales-Nietoa V, Navarro CH, Moreno KJ, Arizmendi-Morquecho A, Chavez-Valdez A, Garcia-Miranda S, et al. Poly(methyl methacrylate)/carbonated hydroxyapatite composite applied as coating on ultra-high molecular weight polyethylene. Prog Org Coat. 2013;76:204–8.
33. Zhu X, Son DW, Ong JL, Kim KH. Characterization of hydrothermally treated anodic oxides containing Ca and P on titanium. J Mater Sci Mater Med. 2003;14:629–34.
34. Narayanan R, Seshadri SK, Kwon TY, Kim KH. Calcium, phosphate-based coatings on titanium and its alloys. J Biomed Mater Res B. 2008;85B:279–99.

35. Goodhew PJ, Humphreys J, Beanland R. Electron microscopy and analysis. 3rd ed. London: Taylor and Francis; 2001. p. 180–200.
36. Dorozhkin SV. A review on the dissolution models of calcium apatites. Prog Cryst Growth Charact. 2002;44:45–61.
37. Xie JH, Luan BL, Wang JF, Liu XY, Rorabeck C, Bourne R. Novel hydroxyapatite coating on new porous titanium and titanium–HDPE composite for hip implant. Surf Coat Technol. 2008;202:2960–8.
38. Jiang HC, Rong LJ. Effect of hydroxyapatite coating on nickel release of the porous NiTi shape memory alloy fabricated by SHS method. Surf Coat Technol. 2006;201:1017–21.
39. BS ISO 13779-2:2000: Implants for surgery—hydroxyapatite—Part 2: coatings of hydroxyapatite. London: British Standards Institution.
40. Thian ES, Huang J, Best SM, Barber ZH, Brooks RA, Rushton N, et al. The response of osteoblasts to nanocrystalline silicon-substituted hydroxyapatite thin films. Biomaterials. 2006;27:2692–8.
41. Eliaz N, Ritman-Hertz O, Aronov D, Weinberg E, Shenhar Y, Rosenman G, et al. The effect of surface treatments on the adhesion of electrochemically deposited hydroxyapatite coating to titanium and on its interaction with cells and bacteria. J Mater Sci Mater Med. 2011;22:1741–52.
42. Zhao XZ, Li HJ, Chen MD, Li KZ, Wang B, Xu ZW, et al. Strong-bonding calcium phosphate coatings on carbon/carbon composites by ultrasound-assisted anodic oxidation treatment and electrochemical deposition. Appl Surf Sci. 2012;258:5117–25.
43. Abdal-Hay A, Barakat NAM, Lim JK. Hydroxyapatite-doped poly(lactic acid) porous film coating for enhanced bioactivity and corrosion behavior of AZ31 Mg alloy for orthopedic applications. Ceram Int. 2013;39:183–95.
44. Argade GR, Panigrahi SK, Mishra RS. Effects of grain size on the corrosion resistance of wrought magnesium alloys containing neodymium. Corros Sci. 2012;58:145–51.
45. Kim HS, Yoo SJ, Ahn JW, Kim DH, Kim WJ. Ultrafine grained titanium sheets with high strength and high corrosion resistance. Mater Sci Eng A. 2011;528:8479–85.
46. Mohamed KR, El-Rashidy ZM, Salama AA. In vitro properties of nanohydroxyapatite/chitosan biocomposites. Ceram Int. 2011;37:3265–71.
47. Yugeswaran S, Yoganand CP, Kobayashi A, Paraskevopoulos KM, Subramanian B. Mechanical properties, electrochemical corrosion and in vitro bioactivity of yttria stabilized zirconia reinforced hydroxyapatite coatings prepared by gas tunnel type plasma spraying. J Mech Behav Biomed Mater. 2012;9:22–33.
48. Chatzistavrou X, Zorba T, Chrissafis K, Kaimakamis G, Kontonasaki E, Koidis P. Influence of particle size on the crystallization process and the bioactive behavior of a bioactive glass system. J Therm Anal Calorim. 2006;85:253–9.
49. Medvecky L, Stulajterova R, Parilak L, Trpcevska J, Durisin J, Barinov SM. Influence of manganese on stability and particle growth of hydroxyapatite in simulated body fluid. Colloid Surf A. 2006;281:221–9.
50. Mayer I, Jacobsohn O, Niazov T, Werckman J, Iliescu M, Richard-Plouet M, et al. Manganese in precipitated hydroxyapatites. Eur J Inorg Chem. 2003;7:1445–51.
51. Mayer I, Cuisinier FJG, Popov I, Schleich Y, Gdalya S, Burghaus O, et al. Phase relations between β-tricalcium phosphate and hydroxyapatite with manganese(II): structural and spectroscopic properties. Eur J Inorg Chem. 2006;7:1460–5.
52. Armulik A, Svineng G, Wennerberg K, Faessler R, Johansson S. Expression of integrin subunit beta1B in integrin beta1-deficient GD25 cells does not interfere with alphaVbeta3 functions. Exp Cell Res. 2000;254:55–63.
53. Bae YJ, Kim MH. Manganese supplementation improves mineral density of the spine and femur and serum osteocalcin in rats. Biol Trace Elem Res. 2008;124:28–34.